Variable Impedance Control for pHRI:

Impact on Stability, Agility, and Human Effort

in Controlling a Wearable Ankle Robot

by

James Arnold

A Thesis Presented in Partial Fulfillment
of the Requirements for the Degree
Master of Science

Approved April 2021 by the
Graduate Supervisory Committee:

Hyunglae Lee, Chair
Spring Berman
Sze Zheng Yong

ARIZONA STATE UNIVERSITY

May 2021

ABSTRACT

This paper introduces a variable impedance controller which dynamically modulates both its damping and stiffness to improve the trade-off between stability and agility in coupled human-robot systems and reduce the human user's effort. The controller applies a range of robotic damping from negative to positive values to either inject or dissipate energy based on the user's intent of motion. The controller also estimates the user's intent of direction and applies a variable stiffness torque to stabilize the user towards an estimated ideal trajectory. To evaluate the controller's ability to improve the stability/agility trade-off and reduce human effort, a study was designed for human subjects to perform a 2D target reaching task while coupled with a wearable ankle robot. A constant impedance condition was selected as a control with which to compare the variable impedance condition. The position, speed, and muscle activation responses were used to quantify the user's stability, agility, and effort, respectively. Stability was quantified spatially and temporally, with both overshoot and stabilization time showing no statistically significant difference between the two experimental conditions. Agility was quantified using mean and maximum speed, with both increasing from the constant impedance to variable impedance condition by 29.8% and 59.9%, respectively. Effort was quantified by the overall and maximum muscle activation data, both of which showed a ~10% reduction in effort. Overall, the study demonstrated the effectiveness of the variable impedance controller.

ACKNOWLEDGMENTS

First, I would like to thank Dr. Hyunglae Lee for his guidance and support during my time at ASU. Dr. Lee has been an extremely influential mentor in my life who has taught me so much about engineering, robotics, and academia. His encouragement and helpfulness have supported me for the past three years and will continue to inspire me as I pursue my Ph.D. Dr. Lee has been an important role model in my life, and I will be forever grateful for his mentorship.

I must also express my appreciation for all of my lab mates at the ASU Neuromuscular Control and Human Robotics Laboratory, who have worked alongside me in the lab and graciously participated in my experiments. I am especially appreciative of Harrison, Eric, and Connor who have worked with me on the Anklebot projects. I am extremely lucky to have had the opportunity to be a part of the lab and work with so many amazing students.

Finally, I would like to thank all of my family and friends who have been so encouraging and supportive. I am forever grateful to my mom, my dad, Michelle, and Ryan for their love, support, and all the quality time we have been able to spend together over the last year. I must also thank Kaan, Matt, and Brett for being such great friends, and I look forward to our trips and Fuzz Buckets' reunion tours in the future. I would also like to express my appreciation for Joyce, who I have shared so many memories and adventures with. Her kindness, sincerity, intelligence, and work ethic have guided me and continue to inspire me every day.

This work was supported by National Science Foundation Awards #1846885 and #1925110.

TABLE OF CONTENTS

Page

LIST OF FIGURES

CHAPTER 1

INTRODUCTION

The study of physical human-robot interaction (pHRI) has found many applications that complement the growing field of research. Applications of pHRI span a wide array of domains such as industry (Cherubini et al., 2016), military (Korpela & Walker, 2018), and rehabilitation (Quintero et al., 2012). This range of application domains necessitates research focused on improving the current control strategies for pHRI.

The human user's safety is the main consideration of any human-robot system, which leads to the question of how to ensure stability. One approach that ensures stability is impedance control that adds positive (dissipative) damping to the system at the interaction point (Colgate, 1988; Lee & Hogan, 2016). By dissipating energy input to the system through positive damping, the robot and overall coupled system are stable. This conservative design approach is popular in pHRI due to the ensured stability (Hannaford & Ryu, 2002; Ott et al., 2008). However, the addition of positive damping to the system can reduce the user's agility and require additional human effort. Therefore, improving the stability/agility trade-off is an active research area within the field of pHRI (Hogan & Buerger, 2005; Newman, 1992).

Research on improving the stability/agility trade-off in pHRI through impedance control has often focused on online modulation of the robotic damping parameter to allow for improved agility and ensured stability. One approach to tune the robotic damping is through demonstration: allowing human users to show the robot the desired task, and then tuning the damping to help the user with this task (Gribovskaya et al.,

2011). A less task-specific approach is to use some quantification of user intent, such as acceleration (Ficuciello et al., 2015; Ikeura & Inooka, 1995), force at the interaction point (Duchaine & Gosselin, 2007; Ranatunga et al., 2015), or muscle activation (Hanafusa & Ishikawa, 2020), to modulate the damping. However, this previous research does not consider the human's inherent damping in the design of the impedance controller.

Additionally, previous research on the design of variable impedance controllers for pHRI does not consider modulating both the damping and stiffness components of the controller based on the user's intent. In the work presented by Bae et al. (2015), the stiffness component is considered for the purpose of collision avoidance with the outside environment, but only the damping component is a function of the user's intent. Finally, previous research only compares the stability/agility effects of the controller but not the effects on human effort.

The goal of this paper is to propose a variable impedance controller that takes into account the inherent human damping and modulates both robotic damping and stiffness. A highly back-drivable wearable ankle robot (Roy et al., 2009) was used to test this variable impedance controller. The ankle joint is of interest for pHRI applications due to the importance of the ankle in common tasks: stability (anteroposterior/mediolateral), lower-limb coordination, shock absorption, and propulsion (Lee et al., 2016; Neptune et al., 2001; Winter et al., 2001). The robotic ankle joint system includes the damping contributions of both the ankle and robot. With knowledge of the ankle's inherent positive damping, a robot can safely apply negative damping while maintaining a stable system. This paper focuses on how and when to apply negative damping, and what other

impedance parameters, such as stiffness, can also be modulated to improve the human user's response.

A preliminary study was performed by the author that focused on variable damping for 1D motion of the ankle (Arnold et al., 2019) and further research demonstrated the applicability of this 1D variable damping controller to the upper limb (Bitz et al., 2020). However, previous studies did not use a full, multi-degree-of-freedom variable impedance controller that modulates damping and stiffness. There are two main hypotheses of this paper: 1) the variable impedance controller can improve the stability/agility trade-off, and 2) the variable impedance controller can reduce human effort. These hypotheses were tested with an experiment where subjects performed a 2D target reaching task requiring ankle motion in the sagittal (dorsiflexion/plantarflexion) and frontal (inversion/eversion) planes.

CHAPTER 2

METHODS

A. Variable Impedance Controller

Since 2D motions of the ankle are considered in the implementation of this controller, vector quantities are used and indicated in bold. Dorsiflexion/plantarflexion (DP) motion is taken to be in the $\pm\hat{\jmath}$ direction, and inversion/eversion (IE) motion in the $\pm\hat{\imath}$ direction. Both directions were considered simultaneously in the study to ensure the controller is suitable for complex, multi-degree-of-freedom pHRI applications.

The variable impedance controller modulates robotic damping ($\boldsymbol{B_r}$) and stiffness (K_r) to help the human user perform a desired motion. The controller can be described by the applied robotic torque, $\boldsymbol{\tau}$, at any given time (Eq. (1)):

$$\boldsymbol{\tau}(\boldsymbol{\theta}, \dot{\boldsymbol{\theta}}) = \boldsymbol{B_r}\,\dot{\boldsymbol{\theta}}(t) + K_r\left(\boldsymbol{\theta}(t) - \mathrm{proj}_{\boldsymbol{\theta_{eq}}}\,\boldsymbol{\theta}(t)\right) + \boldsymbol{g} \tag{1}$$

where $\boldsymbol{\theta}$ is the displacement, $\dot{\boldsymbol{\theta}}$ is the velocity, $\boldsymbol{\theta_{eq}}$ is an equilibrium displacement required for applying stiffness torque, and $\boldsymbol{g}$ is a gravity compensation torque. Angular kinematic quantities are considered since the robotic ankle joint is studied in this paper. Given that $\boldsymbol{\theta}(t) = \theta_{IE}\hat{\imath} + \theta_{DP}\hat{\jmath}$, $\mathrm{proj}_{\boldsymbol{\theta_{eq}}}\,\boldsymbol{\theta}(t)$ is interpreted as the vector projection of $\boldsymbol{\theta}(t)$ onto $\boldsymbol{\theta}_{eq}$. In the wearable ankle robot implementation, where gravity acts downwards on the ankle, a constant torque g_{DP} is applied in the $+\hat{\jmath}$ direction so that $\boldsymbol{g} = g_{DP}\hat{\jmath}$.

To identify the robotic impedance parameters, the controller uses information about the human user's motion through the kinematic data collected by the robot. In the example of the robotic ankle joint, the wearable robot collects the kinematic data from the user as they move their ankle, and the controller simultaneously changes the impedance parameters of the robot to promote stable and agile motion. If the kinematic data indicates that the user is speeding up, the controller will alter its impedance parameters to promote motion in the correct direction. And as the user slows down to reach their desired position, the controller will also react by altering its impedance parameters. Therefore, acceleration is the main kinematic quantity of interest used in determining the intent of motion: the sign of the acceleration can be used to determine whether the intent of motion is positive or negative. However, it is helpful to multiply the acceleration by velocity, since this product has a physical significance as a scaled version of the change in kinetic energy. The product of velocity and acceleration, $\dot{\theta}\ddot{\theta}$, will be used to denote the intent of motion.

This quantification of the user's intent of motion can be directly used to alter robotic damping. With the knowledge that the human ankle joint has inherent positive damping, the variable impedance controller can safely apply negative damping as long as the magnitude of the negative robotic damping is less than the magnitude of the inherent human ankle damping. Therefore, when $\dot{\theta}\ddot{\theta} > 0$, negative robotic damping can be applied by the controller to aid the user's motion by injecting energy into the system. When $\dot{\theta}\ddot{\theta} < 0$, it is beneficial for the controller to provide positive robotic damping that allows the user to reach their desired target in a controlled fashion. A smooth transition from negative to positive damping is desirable, so a logistic function, B, is selected to

transition over the full range of robotic damping (Eq. (2)). A piecewise logistic function is chosen so that the robotic damping at $\dot{\theta}\ddot{\theta} = 0$ can be selected (denoted as b_C).

$$B(\dot{\theta}\ddot{\theta}) = \begin{cases} \dfrac{2b_{LB}}{1 + e^{-k_p\dot{\theta}\ddot{\theta}}} - b_{LB} + b_C, & \dot{\theta}\ddot{\theta} \geq 0 \\ -\dfrac{2b_{UB}}{1 + e^{-k_n\dot{\theta}\ddot{\theta}}} + b_{UB} + b_C, & \dot{\theta}\ddot{\theta} < 0 \end{cases} \tag{2}$$

where k_p and k_n are two tuning parameters which are calculated based on the typical maximum and minimum values of $\dot{\theta}\ddot{\theta}$ (Eq. (3)). Without these tuning parameters, B may not yield values within the full range of robotic damping $[b_{LB} + b_C,\ b_{UB} + b_C]$, which is desired to see the full effects of both the positive and negative damping conditions.

$$k_p = \frac{-ln\left(\frac{1-s}{1+s}\right)}{\dot{\theta}\ddot{\theta}_{max}}, \qquad k_n = \frac{-ln\left(\frac{1+s}{1-s}\right)}{\dot{\theta}\ddot{\theta}_{min}} \tag{3}$$

where $\dot{\theta}\ddot{\theta}_{max}$ is the maximum $\dot{\theta}\ddot{\theta}$ during regular movement, $\dot{\theta}\ddot{\theta}_{min}$ is the minimum $\dot{\theta}\ddot{\theta}$ during regular movement, and s is the sensitivity of the change in robotic damping.

In the wearable ankle robot implementation, damping must be applied in both the DP and IE directions. By calculating $\dot{\theta}\ddot{\theta}_{DP}$ and $\dot{\theta}\ddot{\theta}_{IE}$ independently, $\boldsymbol{B_r}$ can be found as a 2×2 diagonal matrix (Eq. (4)).

$$\boldsymbol{B_r} = \begin{bmatrix} B_{IE} & 0 \\ 0 & B_{DP} \end{bmatrix} \tag{4}$$

The author's previous studies on variable damping control found that once such a controller is used to complete tasks that require more than a single degree-of-freedom (DOF), the application of negative damping during acceleration can cause the human user to deviate from their initial direction of motion towards a target position. While negative damping is effective in helping the user move quickly with little effort, it has no guarantee of helping the user move in the direction that they intend to move, which can become more difficult for the user as energy is injected into the system. Therefore, the variable impedance controller also uses robotic stiffness to prevent users from deviating from their initial intent of direction.

The variable stiffness term in Eq. (1) is dependent on identifying the user's intent of direction, since the intent of direction is used as $\boldsymbol{\theta}_{eq}$, which determines the equilibrium trajectory about which to apply an orthogonal stiffness torque. $\boldsymbol{\theta}_{eq}$ is calculated by using $\dot{\theta}\ddot{\theta}$ to identify the time period when the user is most confident about their direction, is starting to accelerate in this direction, and is not yet experiencing significant negative robotic damping. Any time when $\dot{\theta}\ddot{\theta} > 0$ first becomes true corresponds to this time period, so the position data around this time can be used to calculate $\boldsymbol{\theta}_{eq}$.

The sum of intent of motion in each direction, $\dot{\theta}\ddot{\theta}_{sum} = \dot{\theta}\ddot{\theta}_{IE} + \dot{\theta}\ddot{\theta}_{DP}$, is used as the intent of motion when calculating $\boldsymbol{\theta}_{eq}$ since 2D motion is considered. There are two main cases when $\dot{\theta}\ddot{\theta}_{sum} > 0$ becomes true during typical movement: (1) at the start of motion and (2) when accelerating after slowing down to make a turn/correction.

Figure 1

Illustration of the Calculation of $\boldsymbol{\theta_{eq}}$

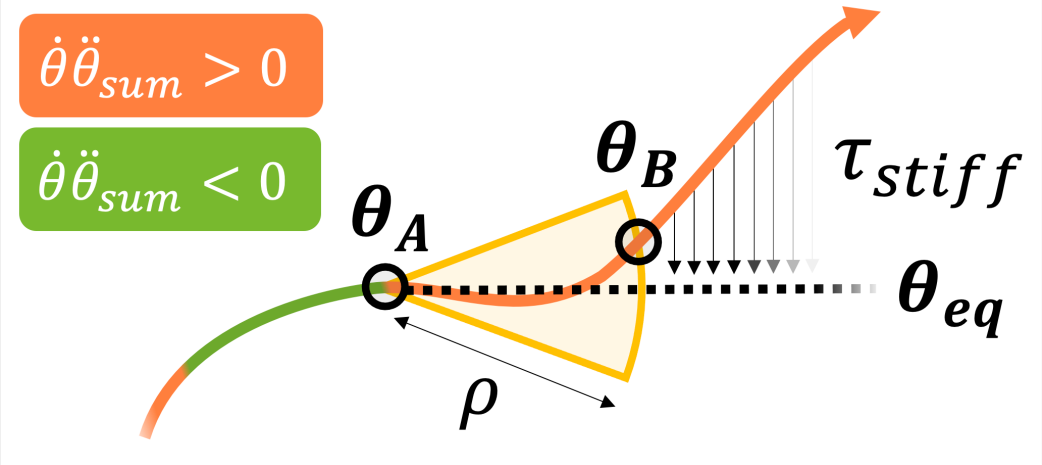

Note. Illustration of the calculation of $\boldsymbol{\theta_{eq}}$ given a hypothetical trajectory represented by an orange/green path. Positive $\dot{\theta}\ddot{\theta}_{sum}$ is shown in orange, negative $\dot{\theta}\ddot{\theta}_{sum}$ in green. The region of data used to calculate $\boldsymbol{\theta_{eq}}$ is shown as a yellow sector of radius ρ, and the $\boldsymbol{\theta_{eq}}$ is shown as a dashed line. Stiffness torque ($\boldsymbol{\tau_{stiff}}$) is shown as a black vector plot.

Therefore, $\boldsymbol{\theta}_{eq}$ is calculated at the start of motion and can also be updated each time the user's intent of direction changes after making a turn.

The amount of position data used to determine $\boldsymbol{\theta}_{eq}$ is dependent on the implementation of the variable impedance controller, and this paper introduces a simple, tunable method effective for point-to-point target reaching tasks. A graphical representation of the method for calculating $\boldsymbol{\theta}_{eq}$ is shown in Fig. 1. $\boldsymbol{\theta_{eq}}$ is found by performing linear regression for all $\boldsymbol{\theta}$ positions between $\boldsymbol{\theta_A}$ and $\boldsymbol{\theta_B}$, where $\boldsymbol{\theta_A}$ is the first $\boldsymbol{\theta}$ position when $\dot{\theta}\ddot{\theta}_{sum} > 0$ becomes true and remains true for all timesteps until $\boldsymbol{\theta_B}$ is defined, $\boldsymbol{\theta_B}$ is the first $\boldsymbol{\theta}$ position when $\overline{\boldsymbol{\theta_A\theta_B}}$ (the distance between $\boldsymbol{\theta_A}$ and $\boldsymbol{\theta_B}$) is $\geq \rho$, and ρ is a tunable parameter which represents the desired $\overline{\boldsymbol{\theta_A\theta_B}}$ that must be traveled for the controller to initialize or update $\boldsymbol{\theta}_{eq}$.

Figure 2

Simulation of the Variable Impedance Controller in 2-DOF

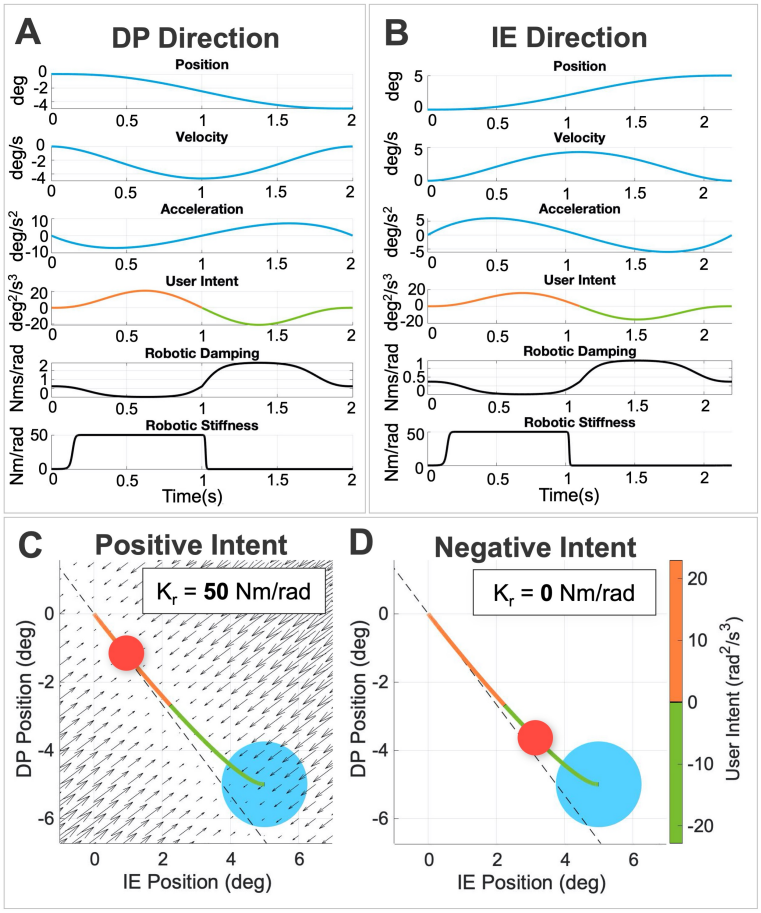

Note. Simulation of the robotic ankle performing a target reaching task. **A-B:** Simulated motion in the plantarflexion (A) and eversion (B) directions. Positive $\dot{\theta}\ddot{\theta}$ is shown in orange, negative $\dot{\theta}\ddot{\theta}$ in green, and robotic impedance in black. **C-D**: 2D trajectory of ankle position at two different times, with current position shown as a red cursor, target position as a blue circle, and path as an orange/green line. A high orthogonal stiffness torque was applied when $\dot{\theta}\ddot{\theta}_{sum}$ was positive, with the resulting restoring torque based on stiffness shown as a vector plot of black arrows and $\boldsymbol{\theta_{eq}}$ shown as a dashed line (C). Zero stiffness was applied when $\dot{\theta}\ddot{\theta}_{sum}$ was negative (D).

The final consideration for implementing variable stiffness is the calculation of K_r. As is desirable for the variable damping equation, the variable stiffness equation

should smoothly transition from a lower bound to an upper bound, with a lower bound of zero and upper bound of k_{UB} (Eq. (5)).

$$K_r\left(\dot{\theta}\ddot{\theta}_{sum}\right) = \frac{k_{UB}}{1 + e^{-r\dot{\theta}\ddot{\theta}_{sum}+\delta}} \tag{5}$$

where k_{UB} is the upper bound of stiffness the controller will apply, r is a sensitivity constant determining how quickly to transition from 0 to k_{UB} stiffness, and δ is a shifting constant used to set the minimum value of $\dot{\theta}\ddot{\theta}_{sum}$ at which the stiffness begins to increase. The sensitivity and shifting parameters must be tuned based on the typical range of $\dot{\theta}\ddot{\theta}_{sum}$ values during regular movement. The goal of tuning these parameters is to ensure that zero stiffness is applied when $\dot{\theta}\ddot{\theta}_{sum} < 0$ since this is when users are setting their direction, and a high stiffness is applied when $\dot{\theta}\ddot{\theta}_{sum} \gg 0$, when users are experiencing high negative damping and need the most assistance in maintaining their desired direction.

A simulation was performed to verify the effectiveness of the variable impedance controller in a 2D target reaching task. Two separate minimum jerk trajectories (Flash & Hogan, 1985) were generated to simulate ankle position profiles with 5° motion in the plantarflexion and eversion directions. All other parameters were selected to be the same as those described in the following section. The results of this simulation can be seen in Fig. 2 and show that $\dot{\theta}\ddot{\theta}$ was used to calculate both variable damping and stiffness. Based on the $\boldsymbol{\theta}_{eq}$ calculated at the start of movement, a guiding stiffness torque was applied.

Figure 3

Experimental Setup and GUI

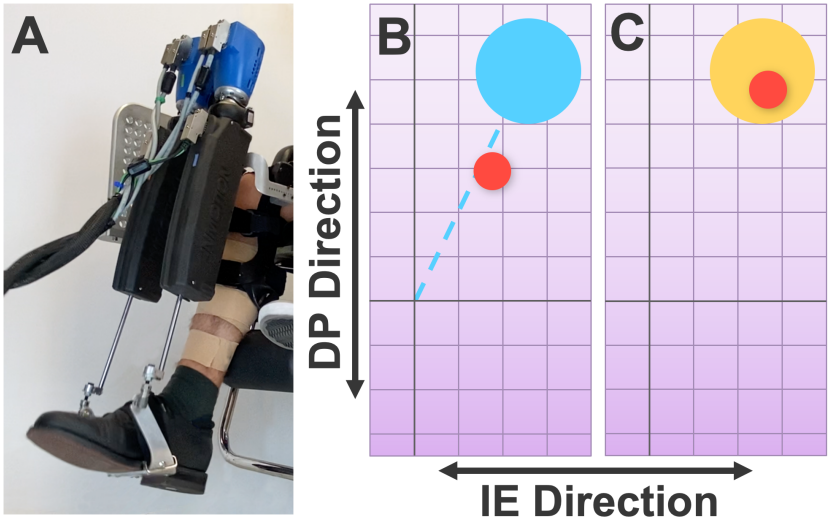

Note. Experimental Setup and GUI. **A:** Anklebot coupled to a subject's ankle. **B:** GUI used for target reaching experiment. Cursor signified by a red circle; targets signified by blue circles. A blue dashed line represented the straightest path between the previous target and the next. **C:** Once a subject reached the target position, the target became orange as a visual indication that they were inside the target.

This simulation did not take into account the dynamics of the human ankle or the effects of motor learning, so experiments were used to evaluate the controller's effectiveness.

B. Experimental Protocol

To evaluate the effectiveness of the variable impedance controller, experiments were performed with a wearable ankle robot, called the Anklebot (Bionik Laboratories Corp., Canada). The wearable robot can apply impedance in 2 DOFs of the human ankle joint, which allows for testing of the controller in the DP and IE directions.

A total of 10 young, healthy subjects (age: 20–27, weight: 47–87 kg, sex: 5 male/5 female) participated in the study, which was approved by the Institutional Review Board of Arizona State University (STUDY00012606). All subjects provided written consent prior to participation and were not informed of the hypothesis.

For each experiment, the subject was required to complete a series of point-to-point target reaching tasks while wearing the Anklebot. Before the robot was coupled to the subject's ankle, surface electromyography (EMG) muscle sensors were placed on the leg and maximum voluntary contraction (MVC) data was collected for the four muscles of interest: tibialis anterior (TA), peroneus longus (PL), soleus (SL), and medial gastrocnemius (MG). Next, the subject sat down, and a knee brace was fitted to the subject's leg. The Anklebot was then attached to the knee brace and connected to joints on the subject's shoe (Fig. 3A). The robot was then calibrated to the neutral position of the human ankle at 90° from the shank in the sagittal plane. Then, gravity compensation was performed on the ankle, so the robot applied a constant, upward torque ($\boldsymbol{g}$) to counteract gravity to reduce fatigue in the subject. At this point, the subject's attention was brought to a graphical user interface (GUI) that showed the current position of the ankle. The subject was told that targets would appear on the GUI, and their goal was to move as quickly and continuously as possible to the target while avoiding overshoot. The GUI provided visual cues on the straightest path between one target to the next (Fig. 3B) and when the subject was inside of the target position (Fig. 3C). The subject had to stay within ±1.5° of the target position for a continuous 2 seconds for the trial to be considered complete.

Over the course of the study, each subject was required to complete 220 target reaching trials. The trials were split into 22 blocks of 10 trials each with a 1-minute break between each block. The first 6 blocks focused on tuning the constants used for calculating variable damping ($\boldsymbol{B_r}$). The first 3 blocks only required motion in the frontal plane to tune the variable damping constants for motion in the IE direction, $k_{p,IE}$ and $k_{n,IE}$. The second set of 3 blocks only required motion in the sagittal plane to tune the variable damping constants for motion in the DP direction, $k_{p,DP}$ and $k_{n,DP}$. Following the tuning blocks, there were 2 practice blocks that introduced each subject to the 2D target reaching task. The remaining 14 blocks required the subject to perform the 2D target reaching task and were the blocks used for data analysis.

During the tuning blocks, each trial required a motion of ±15° in the DP direction or ±7.5° in the IE direction, and then a return to the neutral position between trials. These distances were selected to cover the full range of motion required for the study. A high orthogonal stiffness torque was used to limit the subject's movement to the plane of motion being tuned. For each set of 3 blocks within the tuning session, the first block applied zero robotic damping, and the average $\dot{\theta}\ddot{\theta}_{max}$ and $\dot{\theta}\ddot{\theta}_{min}$ values were used to calculate an initial estimate of the tuning constants k_p and k_n. The second block applied variable damping with the tuning constants found in the previous block and calculated a new set of constants. Finally, a third block used the tuning constants calculated in the second block to find the final values of k_p and k_n used in the study. By the end of the 6 tuning blocks, the constants $k_{p,DP}$, $k_{n,DP}$, $k_{p,IE}$, and $k_{n,IE}$ were found and used throughout the remainder of the study.

The remaining blocks (referred to as the *main blocks*) required subjects to perform a more complicated 2D target reaching task. Each target required that the subject move their ankle in both the DP and IE directions, with targets at a distance of ±5–10° in the DP direction and ±2.5–5° in the IE direction. Targets were generated within an elliptical region around the neutral position with defined limits at ±15° in the DP direction and ±7.5° in the IE direction. The ranges of target distances were selected to promote an unpredictable path within the elliptical region and to limit the variability in distances between targets to simplify the data analysis. Each block can be considered as a path the subject must follow, with the locations of the 10 trials/targets defining the path. Four random paths meeting the aforementioned criteria were generated and used throughout the experiment.

A small, constant positive damping with zero stiffness condition—referred to throughout the remainder of this paper as *constant impedance*—is the experimental control condition used to understand the effects of the variable impedance controller on the human user's ability to perform the target reaching task. In this condition, the positive damping was set to a constant 3 Nms/rad in the DP direction and 1.5 Nms/rad in the IE direction. The magnitudes of constant positive damping selected in this implementation are small and were selected to prevent subjects from experiencing large overshoots that would occur if constant zero damping were applied. The values used in this experiment were based on the author's preliminary 1D variable damping experiments (Arnold et al., 2019). The same positive damping limits were set to the upper bounds of damping ($b_{UB} + b_C$) in the variable impedance condition, and the lower bounds of the damping range ($b_{LB} + b_C$) were set to -1.5 Nms/rad in the DP direction and -0.5 Nms/rad in the IE

direction. These lower bounds were selected based on the known inherent positive damping in the human ankle, quantified in the previous work (Lee et al., 2014; Lee & Hogan, 2015). The variable damping logistic function was set to have a damping (b_C) of 0.25 Nms/rad when $\dot{\theta}\ddot{\theta} = 0$, and the sensitivity constant was set to $s = 0.95$ to ensure that $B_r = 0.95b_{LB} + b_C$ at $\dot{\theta}\ddot{\theta}_{max}$ and $B_r = 0.95b_{UB} + b_C$ at $\dot{\theta}\ddot{\theta}_{min}$.

The maximum stiffness (k_{UB}) of the variable impedance controller was set to 50 Nm/rad, a value selected based on previous work of characterizing ankle impedance during dynamic tasks (Lee et al., 2014). From the user intent data collected from the author's previous experiments requiring a similar target reaching task, the other constants required to define K_r were pre-tuned to ensure subjects experienced the full range of stiffness during normal movement (Arnold et al., 2019). A sensitivity constant of $r = 2.75$ was selected so that the transition from $0.05k_{UB}$ to $0.95k_{UB}$ occurred over a range of ~2 rad^2/s^3, which allowed for a smooth transition from 0 to 50 Nm/rad during a typical target reaching trial. Additionally, a shifting constant of $\delta = 6$ was selected so that $0.05k_{UB}$ corresponded with $\dot{\theta}\ddot{\theta} \approx 1$ rad^2/s^3, the selected positive value of intent when it was desirable to start applying noticeable stiffness, as was determined through analysis of the data collected in the author's previous work (Arnold et al., 2019) and preliminary experiments with 2D variable damping. As is presented later in the *Results* section of this paper, this manual tuning of the stiffness parameters was successful in using the full range of stiffness (Fig. 5). $\boldsymbol{\theta}_{eq}$ was calculated when both $\dot{\theta}\ddot{\theta}_{sum} > 0$ became true and the subject had moved 5% of the range of motion used in this study, i.e., $\rho = 0.05\sqrt{15^2 + 7.5^2}°$.

Figure 4

Visual Representations of the Performance Metrics

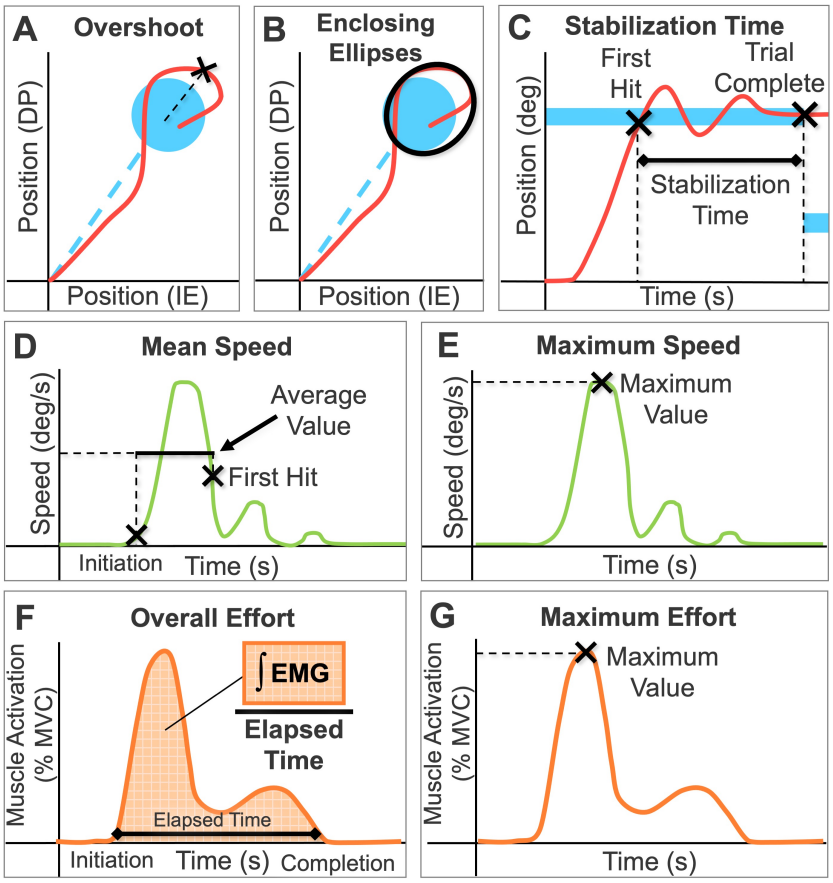

Note. Visual representations of the performance metrics. Row 1 shows stability performance metrics (position response in red), row 2 agility (velocity response in green), and row 3 effort (EMG response in orange). Target positions for position responses shown in blue.

Either variable impedance or constant impedance was applied for each of the main blocks. The main blocks used for data analysis were grouped together by impedance condition into sets of 3 and 4 blocks to give subjects time to acclimate to the different impedance conditions.

C. Data Analysis

The kinematic and EMG data collected while subjects interacted with the variable impedance condition was compared with the data from the constant impedance condition to determine if there was a statistically significant benefit of the variable impedance controller. Various performance metrics were used to quantitatively analyze the effects of the variable impedance controller and can be organized into three categories: stability, agility, and effort.

Stability was quantified using performance metrics that focused on the position response of the subjects throughout each target reaching trial. Three metrics were defined to quantify the stability of a trial: overshoot, enclosing ellipses, and stabilization time. *Overshoot* was defined as the maximum tangential distance past the target position at any point throughout a trial (Fig. 4A). *Enclosing ellipses* was defined as the area of the smallest ellipse that could fit the position data collected after the subject first hit the target (Fig. 4B), with the smallest ellipse determined by the Khachiyan Algorithm for finding minimum volume ellipsoids (Todd & Yildirim, 2007). *Stabilization time* was defined as how long it took the subject to complete a trial once they first hit the target (Fig. 4C).

Agility was quantified using performance metrics that analyzed the speed in which subjects were able to complete each target reaching task. Speed metrics were selected over time metrics (e.g., task completion time) since time metrics are not well suited to the variable distance target reaching task considered in this study. There were two metrics used to quantify agility: mean and maximum speed. The *mean speed* was defined as the average speed calculated between when the subject initiated motion to

when they first hit the edge of the target (Fig. 4D). The initiation time was defined as the time when the ankle position moved 2°, which helped account for errors in calculation due to small movements a subject can make within the previous target location. The *maximum speed* was defined as the highest magnitude speed the subject reached at any time during the trial (Fig. 4E).

Effort was quantified using performance metrics that aggregated the collected EMG data to evaluate the amount of muscle activation required to complete each target reaching task. Before calculating any performance metrics, the raw EMG data was demeaned, rectified, filtered using a 4^{th} order Butterworth low-pass filter with a cutoff frequency of 5 Hz, and scaled by MVC. With this processed EMG data, the effort was quantified with two metrics: overall effort and maximum effort. *Overall effort* was defined by first integrating the processed EMG data over the time from the start of motion to the end of motion for each trial, then taking the sum of all trials for which that muscle was relevant to motion, and finally dividing the sum by the elapsed time over which the integrals for each trial were taken (Fig. 4F). Determining which muscle is relevant to motion was based on the movement directions: dorsiflexion trials corresponded to TA muscle data, plantarflexion trials corresponded to the mean of SL and MG data, and eversion trials corresponded to PL data. Inversion motion could not be quantified by surface EMG sensors, so was not considered in the effort analysis. The calculation of the other effort metric, *maximum effort*, followed a similar procedure to overall effort, except that instead of taking a sum of integrals and dividing by time, the maximum value was taken for each trial (Fig. 4G).

For all of the previously described performance metrics, outlier rejection was performed to remove trials that did not follow a typical position response. This outlier rejection procedure was the same for all subjects and required normalizing the position response of all trials in the DP and IE directions, shifting the times of the trials so all trials' position responses were aligned, and then removing trials that fell outside of ±2.5 standard deviation (STD) from the mean position response over time. While no subject was unable to complete a trial due to instability, some trials had position responses that deviated from the typical response. An example of trials that are often removed by this method are those trials at the start of a block after the impedance condition has changed.

Statistical analysis was performed to determine the significance of differences between the variable and constant conditions for each performance metric. Two tailed t-tests were used for all metrics whose data passed the Shapiro–Wilk normality test. All metrics passed the Shapiro–Wilk normality test except the maximum speed metric data. For the maximum speed results, the Wilcoxon signed-rank test was used instead.

CHAPTER 3

RESULTS

The data from the 10 subjects demonstrated that the variable impedance controller could balance the stability/agility trade-off and reduce human effort. Qualitative results of a representative subject and quantitative group results of the 10 subjects are provided in the following subsections. In the interest of conciseness, the variable impedance condition will be referred to as *VI*, and the constant impedance condition will be referred to as *CI*.

A. Representative Results

The representative subject's position profiles for all four movement directions were time shifted so the start of motion (with time 0 corresponding to a movement of 2°) were aligned and normalized (position 0 corresponding to the starting position and ±1 corresponding to the target position). When compared with the average position response from *CI* trials (Fig. 5A), the average *VI* response (Fig. 5B) showed faster settling times to reach 95% of the target position. While this result must be verified for all subjects to establish a statistically significant benefit in the agility of the *VI* controller, further investigation of the representative subject is helpful to verify that the *VI* controller worked as expected. The user intent was calculated as the product of velocity and acceleration of the robotic ankle joint (Fig. 5C) and was then used for the calculation of robotic damping and stiffness. The damping was checked to see if the tuning trials allowed the subject to use the full range of damping (Fig. 5D). Due to variations within the distance traveled during each trial and the subject not always reaching the target in a

Figure 5

Representative Subject Kinematic Results

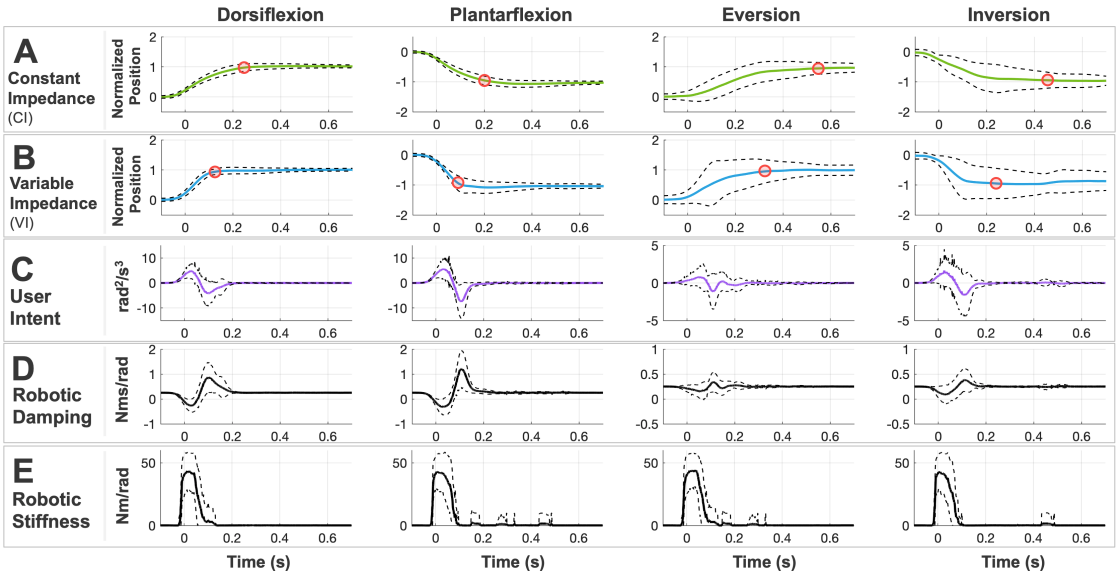

Note. Representative subject kinematic results showing the mean response (solid line) and ±1 STD from the mean (dashed line) of all trials. Position response of *CI* trials shown in green, *VI* position in blue. Settling time to reach 95% of target position indicated in red. User intent during *VI* shown in purple, robotic impedance in black. Each trial's position data was normalized between 0 and ±1 and time shifted to align trials by initiation time.

continuous motion, the mean damping plot did not appear to show the use of the full damping range, but each individual trial typically did use the full range. The stiffness commanded to the robot also showed the use of the full range of stiffness for each trial (Fig. 5E).

For the controller to be effective, the robotic stiffness torque must be applied in the correct direction. However, all subjects experienced outlier trials where the initial $\boldsymbol{\theta}_{eq}$ was not correct and a new $\boldsymbol{\theta}_{eq}$ was calculated. A representative outlier trial is presented to show how the *VI* controller adapted in this situation (Fig. 6). As the subject started moving, the controller applied zero stiffness torque while calculating the initial $\boldsymbol{\theta}_{eq}$ (Fig. 6A) and then applied a high orthogonal stiffness torque (Fig. 6B) while the user's intent

Figure 6

Representative Outlier Trial

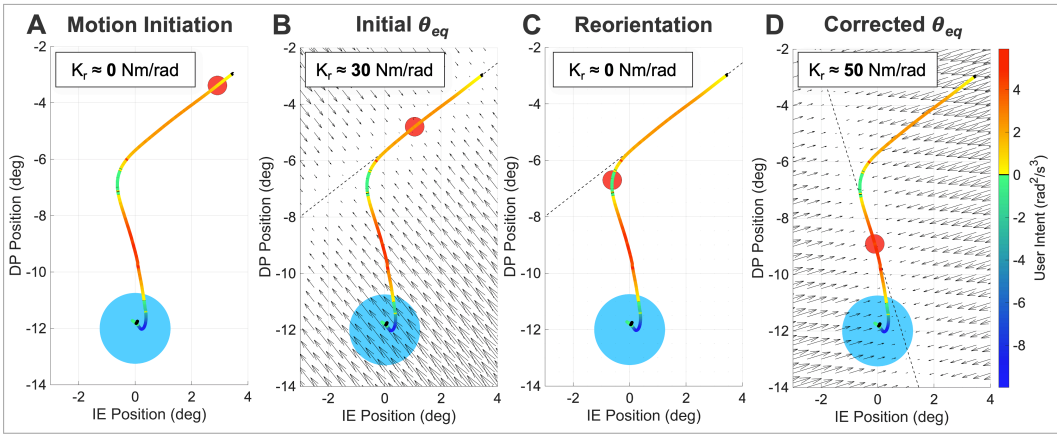

Note. Representative trial demonstrating variable stiffness when the user's intent of direction ($\boldsymbol{\theta}_{eq}$) was initially incorrect.

of motion was positive. However, the subject then slowed down to make a slight correction (Fig. 6C). Once the intent again became positive, a new $\boldsymbol{\theta}_{eq}$ was calculated, allowing for an orthogonal stiffness torque to be applied that guided the user to the target (Fig. 6D).

B. Group Results: Stability

The stability performance metrics demonstrate that the *VI* controller did not cause a significant decrease in each subject's ability to perform the task in a controlled manner. The overshoot metric showed a 13.8% increase from *CI* to *VI*, representing an increase in mean overshoot by 0.08° (Fig. 7A). Based on the results of the paired t-test, there was no statistically significant difference in the overshoots between *CI* and *VI*. The enclosing ellipses metric showed a 23.5% increase from *CI* to *VI*, representing an increase in mean ellipse area of 0.25 deg^2 between the conditions (Fig. 7B). While the paired t-test

Figure 7

Group Results Comparing Constant and Variable Impedance

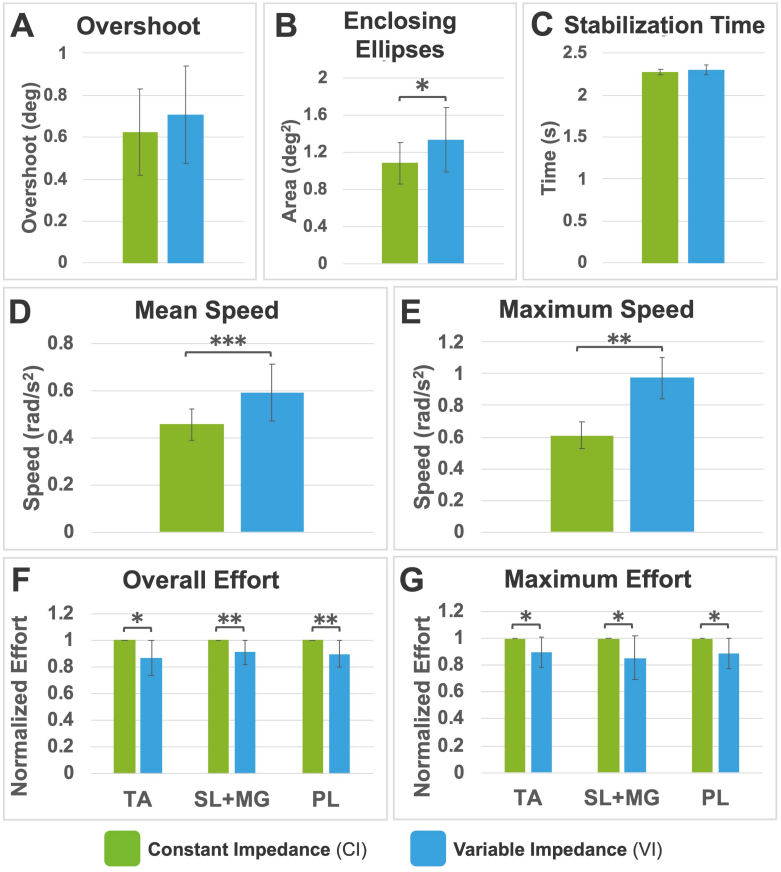

Note. Group results (10 subjects) of the different performance metrics comparing the impedance conditions. Mean is shown by the height of the colored bars and standard deviation between means is shown with error bars. Stars are used to show significance in pairwise comparisons: * for $p < 0.05$, ** for $p < 0.01$, and *** for $p < 0.001$.

indicated this difference to be statistically significant, the difference between the size of the enclosing ellipses does not demonstrate a response with greatly reduced stability. Finally, the stabilization time metric showed a 1.2% increase (0.03 s) in stabilization time from *CI* to *VI*, an increase which was not statistically significant (Fig. 7C). Overall, these metrics found *VI* to have a similar stability response to *CI*.

C. Group Results: Agility

The agility performance metrics show that the *VI* controller allowed the subjects to reach higher speeds than the *CI* controller. The mean speed metric showed a 29.8% increase from *CI* to *VI*, and the paired t-test demonstrated this result to be statistically significant (Fig. 7D). The maximum speed metric showed a 59.9% increase from *CI* to *VI* (Fig. 7E). From the Wilcoxon signed-rank test, this increase in speed was found to be statistically significant. Coupled with the stability performance metric results, these results demonstrate the *VI* controller's ability to balance the stability/agility trade-off.

D. Group Results: Effort

The final set of performance metrics used muscle activation data to show the *VI* controller's ability to reduce the effort required by the user. Due to the inherent intersubject variability in EMG data collection, different subjects had significantly different percent MVC values for the overall and maximum effort metrics. Therefore, all effort metrics were normalized by the magnitude of the effort in the *CI* condition. Then, a t-test was used to check if the effort was statistically different from a value of 1 with unknown variance, with 1 corresponding to the effort in the *CI* condition. During trials requiring either dorsiflexion (TA), plantarflexion (mean of PL and MG), and/or eversion (PL) motion, the overall (Fig. 7F) and maximum (Fig. 7G) effort were reduced by about 10% for all directions. Based on the results of the t-test, both the overall and maximum effort metrics showed a statistically significant decrease in effort from *CI* to *VI*.

CHAPTER 4

DISCUSSION

The author's previous work (Arnold et al., 2019) and other previous research from the author's research group (Bitz et al., 2020) focused on modulating variable damping based on the user's intent, but did not consider a stiffness component. Variable damping control was effective when motion was limited to a single DOF, but most pHRI applications require multiple DOFs. Variable damping alone cannot account for deviation of the user from their initial intent of direction caused by energy injected into the system through negative damping. Therefore, this study incorporates the concept of variable stiffness.

One notable benefit of the controller is its ability to adapt to situations when the user changes their intent of direction. While the point-to-point target reaching task considered in this study typically did not require changes in direction, some of the outlier trials when the subject was learning the task or acclimating to the variable impedance controller demonstrated the controller's ability to adapt to changes in the user's intent of direction, as shown in Fig. 6. Therefore, this controller could potentially be applicable to more complicated tasks that require changes in direction during movement.

Other researchers' work on the implementation of variable impedance/admittance controllers in pHRI systems has shown the ability of their controllers to improve the performance of the coupled human-robot system with regards to a few, task-specific performance metrics, such as reducing completion time in a drawing or maze following task (Ficuciello et al., 2015; Lecours et al., 2012) or quantifying how well a robot's motion matches the minimum jerk trajectory in a cooperative lifting task (Ranatunga et

al., 2015). Unlike previous work, this paper presents the results of many different performance metrics that demonstrate the proposed controller's ability to maintain stability, promote agility, and reduce the user's effort—all three of which are essential considerations in the design of coupled human-robot systems.

Future research will focus on refining the controller and testing it for different pHRI applications. One improvement that can be made to the controller is through more research that focuses on characterizing the impedance properties of the human neuromuscular system during various tasks. Another improvement that can be made to the controller is in the tuning methods. The variable damping range and constants could be tuned more comprehensively to apply the ideal range for each subject, and the tuning method should consider the effects of tasks requiring variable distances, since the current study uses constant distances for tuning trials. The variable stiffness term in the controller could also be tuned to each subject, rather than using the pre-tuned parameters used in the current study, to better ensure the use of the full range of stiffness. Moreover, the quantification of intent of motion used for the stiffness term, $\dot{\theta}\ddot{\theta}_{sum}$, could be reconsidered.

Besides improving the controller, future research will focus on testing the controller in other applications and comparing it to other assistive control techniques. The controller should be tested in a walking study, which will require considerations on the impedance of the environment, analogous to the work presented in Li et al. (2018). Additionally, the ideal trajectory for a walking task will not be a linear, point-to-point path as considered in this study. However, the proposed controller can be adapted to find a curved $\boldsymbol{\theta}_{eq}$, which would promote motion along the intended path and allow for

recalculation of $\boldsymbol{\theta}_{eq}$ for unpredictable walking tasks, while variable damping helps to reduce user effort.

Future research focusing on task-specific applications of the proposed controller, such as walking, will allow for a more comprehensive analysis of the assistive/resistive effects of the controller's damping and stiffness components. One limitation of the current study is that the variability of distances and directions required for each point-to-point target reaching task resulted in inconsistent levels of applied stiffness torque over time, since the deviation from $\boldsymbol{\theta}_{eq}$ varied between trials. However, the stiffness torque provided by the controller in repetitive, task-specific applications would likely be more consistent and allow for a comparison of the effects of the damping and stiffness components of the controller.

That said, the current wearable ankle robot implementation of the controller is directly applicable to rehabilitation applications, where seated target reaching tasks are common, and the proposed controller would be able to help patients with weakened muscles (Forrester, et al., 2011). Testing the controller while coupled with other joints besides the ankle will also be required to verify the general applicability of the controller.

REFERENCES

Arnold, J., Hanzlick, H., & Lee, H. (2019). Variable Damping Control of the Robotic Ankle Joint to Improve Trade-off between Performance and Stability. *Proceedings of 2019 IEEE International Conference on Robotics and Automation*, 1699–1704. https://doi.org/10.1109/ICRA.2019.8793869

Bae, J., Ko, J. H, & Hong, D. (2015). Variable impedance control with stiffness for human-robot cooperation system. *2015 15th International Conference on Control, Automation and Systems (ICCAS)*, 1231–1233. https://doi.org/10.1109/ICCAS.2015.7364818

Bitz, T., Zahedi, F., & Lee, H. (2020). Variable Damping Control of a Robotic Arm to Improve Trade-off between Agility and Stability and Reduce User Effort. *Proceedings of 2020 IEEE International Conference on Robotics and Automation*, 11259–11265. https://doi.org/10.1109/ICRA40945.2020.9196572

Cherubini, A., Passama, R., Crosnier, A., Lasnier, A., & Fraisse, P. (2016). Collaborative manufacturing with physical human–robot interaction. *Robotics and Computer-Integrated Manufacturing*, 40, 1–13. https://doi.org/10.1016/j.rcim.2015.12.007

Colgate, E. (1988) The control of dynamically interacting systems. [PhD Dissertation, Massachusetts Institute of Technology]. MIT Libraries.

Duchaine, V., & Gosselin, C. (2007). General Model of Human-Robot Cooperation Using a Novel Velocity Based Variable Impedance Control. *Second Joint EuroHaptics Conference and Symposium on Haptic Interfaces for Virtual Environment and Teleoperator Systems (WHC'07)*, 446–451. https://doi.org/10.1109/WHC.2007.59

Ficuciello, F., Villani, L., & Siciliano, B. (2015). Variable Impedance Control of Redundant Manipulators for Intuitive Human-Robot Physical Interaction. *IEEE Transactions on Robotics*, 31(4), 850–863. https://doi.org/10.1109/TRO.2015.2430053

Flash, T, & Hogan, N. (1985). The coordination of arm movements: An experimentally confirmed mathematical model. *The Journal of Neuroscience*, 5(7), 1688-1703.

Forrester, L., Roy, A., Krebs, H., & Macko, R. (2011). Ankle Training with a Robotic Device Improves Hemiparetic Gait After a Stroke. *Neurorehabilitation and Neural Repair*, 25(4), 369–377. https://doi.org/10.1177/1545968310388291

Gribovskaya, E., Kheddar, A., & Billard, A. (2011). Motion learning and adaptive impedance for robot control during physical interaction with humans. *Proceedings of 2011 IEEE International Conference on Robotics and Automation*, 4326–4332. https://doi.org/10.1109/ICRA.2011.5980070

Hanafusa, M., & Ishikawa, J. (2020). Human-Adaptive Impedance Control Using Recurrent Neural Network for Stability Recovery in Human-Robot Cooperation. *2020 IEEE 16th International Workshop on Advanced Motion Control (AMC)*, 265–272. https://doi.org/10.1109/AMC44022.2020.9244389

Hannaford, B., & Ryu, J. H. (2002). Time-domain passivity control of haptic interfaces. *IEEE Transactions on Robotics and Automation*, 18(1), 1–10. https://doi.org/10.1109/70.988969

Hogan, N., & Buerger, S. P. (2005). Impedance and interaction control. *Robotics and Automation Handbook*, New York, CRC Press.

Ikeura, R., & Inooka, H. (1995). Variable impedance control of a robot for cooperation with a human. *Proceedings of 1995 IEEE International Conference on Robotics and Automation*, 3, 3097–3102 vol.3. https://doi.org/10.1109/ROBOT.1995.525725

Korpela, C., & Walker, A. (2018). Wearable Technologies for Enhanced Soldier Situational Awareness. *Proceedings of the 2nd International Conference on Vision, Image and Signal Processing*, 1–6. https://doi.org/10.1145/3271553.3271620

Lecours, A., Mayer-St-Onge, B., & Gosselin, C. (2012). Variable admittance control of a four-degree-of-freedom intelligent assist device. *Proceedings of 2012 IEEE International Conference on Robotics and Automation*, 3903–3908. https://doi.org/10.1109/ICRA.2012.6224586

Lee, H., & Hogan, N. (2015). Time-Varying Ankle Mechanical Impedance During Human Locomotion. *IEEE Transactions on Neural Systems and Rehabilitation Engineering*, 23(5), 755-764.

Lee, H., & Hogan, N. (2016) Essential considerations for design and control of human-interactive robots. *Proceedings of 2016 IEEE International Conference on Robotics and Automation*, 3069-3074. https://doi.org/ ICRA.2016.7487472

Lee, H., Krebs, H., & Hogan, N. (2014). Multivariable Dynamic Ankle Mechanical Impedance with Active Muscles. *IEEE Transactions on Neural Systems and Rehabilitation Engineering*, 22(5), 971–981. https://doi.org/10.1109/TNSRE.2014.2328235

Lee, H., Rouse, E., & Krebs, H. (2016). Summary of Human Ankle Mechanical Impedance During Walking. *IEEE Journal of Translational Engineering in Health and Medicine*, 4, 1–7. https://doi.org/10.1109/JTEHM.2016.2601613

Li, H. Y., Paranawithana, I., Liangjing Yang, Lim, T., Shaohui Foong, Foo Cheong Ng, & U-Xuan Tan. (2018). Stable and Compliant Motion of Physical Human–Robot Interaction Coupled with a Moving Environment Using Variable Admittance and Adaptive Control. *IEEE Robotics and Automation Letters*, 3(3), 2493–2500. https://doi.org/10.1109/LRA.2018.2812916

Neptune, R., Kautz, S., & Zajac, F. (2001). Contributions of the individual ankle plantar flexors to support, forward progression and swing initiation during walking. *Journal of Biomechanics*, 34(11), 1387–1398. https://doi.org/10.1016/S0021-9290(01)00105-1

Newman, W. (1992). Stability and Performance Limits of Interaction Controllers. *Journal of Dynamic Systems, Measurement, and Control*, 114(4), 563–570. https://doi.org/10.1115/1.2897725

Ott, C., Albu-Schaffer, A., Kugi, A., & Hirzinger, G. (2008). On the Passivity-Based Impedance Control of Flexible Joint Robots. *IEEE Transactions on Robotics*, 24(2), 416–429. https://doi.org/10.1109/TRO.2008.915438

Quintero, H., Farris, R., & Goldfarb, M. (2012). A Method for the Autonomous Control of Lower Limb Exoskeletons for Persons with Paraplegia. *Journal of Medical Devices*, 6(4), 0410031–0410036. https://doi.org/10.1115/1.4007181

Ranatunga, I., Cremer, S., Popa, D., & Lewis, F. (2015). Intent aware adaptive admittance control for physical human-robot interaction. *Proceedings of 2015 IEEE International Conference on Robotics and Automation*, 5635–5640. https://doi.org/ 10.1109/ICRA.2015.7139988

Roy, A., Krebs, H., Williams, D., Bever, C., Forrester, L., Macko, R., & Hogan, N. (2009). Robot-Aided Neurorehabilitation: A Novel Robot for Ankle Rehabilitation. *IEEE Transactions on Robotics*, 25(3), 569–582. https://doi.org/10.1109/TRO.2009.2019783

Todd, M., & Yildirim, E. (2007). On Khachiyan's algorithm for the computation of minimum-volume enclosing ellipsoids. *Discrete Applied Mathematics*, 155(13), 1731–1744. https://doi.org/10.1016/j.dam.2007.02.013

Winter, D., Patla, A., Rietdyk, S., & Ishac, M. (2001). Ankle Muscle Stiffness in the Control of Balance During Quiet Standing. *Journal of Neurophysiology*, 85(6), 2630–2633. https://doi.org/10.1152/jn.2001.85.6.2630

APPENDIX A

NOTE ON THE PUBLICATION OF THIS WORK

This work was published in *IEEE Robotics and Automation Letters (RA-L)* (2021, 6 (2), 2429-2436, DOI: 10.1109/LRA.2021.3062015) and was also accepted for the presentation at *IEEE International Conference on Robotics and Automation (ICRA 2021)*, May 2021, Xi'an, China. The published work was co-authored by Dr. Hyunglae Lee, who has granted permission to James Arnold to present this work as his thesis.

In reference to IEEE copyrighted material, which is used with permission in this thesis, the IEEE does not endorse any of Arizona State University's products or services. Internal or personal use of this material is permitted.